The Journal of Infectious Diseases

MAJOR ARTICLE

Varicella Zoster Virus Induces Nuclear Translocation of the Neurokinin-1 Receptor, Promoting Lamellipodia Formation and Viral Spread in Spinal Astrocytes

Andrew N. Bubak,[1] Christina N. Como,[1] Anna M. Blackmon,[1] Seth Frietze,[4] Teresa Mescher,[1] Dallas Jones,[1] Randall J. Cohrs,[1,2] Petr Paucek,[1] Nicholas L. Baird,[1] and Maria A. Nagel[1,3]

[1]Department of Neurology, [2]Department of Immunology and Microbiology, and [3]Department of Ophthalmology, University of Colorado School of Medicine, Aurora; and [4]Department of Medical Laboratory and Radiation Sciences, University of Vermont, Burlington

Background. Varicella zoster virus (VZV) can present as a myelopathy with spinal astrocyte infection. Recent studies support a role for the neurokinin-1 receptor (NK-1R) in virus infections, as well as for cytoskeletal alterations that may promote viral spread. Thus, we examined the role of NK-1R in VZV-infected primary human spinal astrocytes (HA-sps) to shed light on the pathogenesis of VZV myelopathy.

Methods. Mock- and VZV-infected HA-sps were examined for substance P (subP) production, NK-1R localization, morphological changes, and viral spread in the presence or absence of the NK-1R antagonists aprepitant and rolapitant.

Results. VZV infection of HA-sps induced nuclear localization of full-length and truncated NK-1R in the absence of the endogenous ligand, subP, and was associated with extensive lamellipodia formation and viral spread that was inhibited by NK-1R antagonists.

Conclusions. We have identified a novel, subP-independent, proviral function of nuclear NK-1R associated with lamellipodia formation and viral spread that is distinct from subP-induced NK-1R cell membrane/cytoplasmic localization without lamellipodia formation. These results suggest that binding of a putative viral ligand to NK-1R produces a dramatically different NK-1R downstream effect than binding of subP. Finally, the NK-1R antagonists aprepitant and rolapitant provide promising alternatives to nucleoside analogs in treating VZV infections, including myelopathy.

Keywords. Varicella zoster virus; myelopathy; astrocytes; neurokinin-1 receptor; lamellipodia; aprepitant; rolapitant.

Varicella zoster virus (VZV) is an exclusively human, ubiquitous alphaherpesvirus that produces varicella, after which it establishes latency in neurons within cranial nerve, dorsal root, and autonomic ganglia [1–3]. With advanced age or immunosuppression, VZV reactivates and typically travels peripherally to skin, producing zoster. However, virus can also travel centrally along nerve fibers to infect the spinal cord, producing myelopathy with or without zoster [4].

VZV myelopathy is one of several neurological complications of VZV reactivation and presents as a self-limiting paraparesis with or without sensory features and sphincter problems [4]. In immunocompromised individuals, particularly those with human immunodeficiency virus infection, myelopathy can be progressive and fatal, with frank virus infection of the spinal cord [5, 6]. Pathogenic mechanisms of VZV myelopathy are not well characterized, mainly because VZV is an exclusively human virus. However, postmortem analyses of 8 patients with VZV myelopathy revealed that astrocytes, as well as oligodendrocytes and neurons, in the spinal cord were infected horizontally and longitudinally [7]. The site of cord involvement was associated with VZV reactivation and zoster, supporting the notion that, following reactivation from ganglionic neurons, VZV travels peripherally to the skin, producing zoster, and centrally to the spinal cord, producing myelopathy. Additional support that VZV myelopathy can be caused by direct VZV invasion of the spinal cord is clinical improvement following acyclovir therapy in cases of (1) acute and rapidly progressive, virologically verified VZV myelopathy in patients with acquired immunodeficiency syndrome [8, 9] and (2) acute VZV myelopathy in patients with multiple sclerosis who are receiving immunomodulatory therapy [10, 11].

Of the cell types within the spinal cord, astrocytes are most likely key contributors to central nervous system (CNS) spread of infection and development of VZV myelopathy, since astrocytes are the most abundant glial cell type in the CNS, are crucial regulators of extracellular homeostasis and neuroinflammation, and have a high capacity for migration [12]. Current knowledge of VZV infection of astrocytes is limited to human cortical astrocytes. Postmortem immunohistochemical studies of a brain with VZV encephalitis show that cortical astrocytes are

Received 13 February 2018; editorial decision 11 May 2018; accepted 14 May 2018; published online May 19, 2018.

Correspondence: M. A. Nagel, MD, Department of Neurology, University of Colorado School of Medicine, 12700 E 19th Ave, Mail Stop B182, Aurora, CO 80045 (maria.nagel@ucdenver.edu).

The Journal of Infectious Diseases® 2018;218:1324–35

DOI: 10.1093/infdis/jiy297

preferentially infected [13–15]. In vitro studies show that astrocytes isolated from human brain are permissive to VZV infection [16] and have decreased expression of glial fibrillary acidic protein (GFAP) [17].

Previous studies have shown that binding of substance P (subP) to the neurokinin-1 receptor (NK-1R) is involved in human immunodeficiency virus infection, measles, and respiratory syncytial virus infection [18–20] and contributes to cytoskeletal rearrangements and membrane blebbing [21] that may facilitate VZV spread [22]. NK-1R is a G-protein–coupled tachykinin receptor expressed as a full-length or truncated form on the surface of many cells and is involved in pain transmission, immune modulation, and multiple cellular processes [23, 24].

Herein, we tested whether primary human spinal cord astrocytes are permissive to VZV infection, providing an in vitro model to study VZV myelopathy pathogenesis. We also tested whether VZV infection of primary human spinal astrocytes produces subP and whether blockade of NK-1R inhibits VZV-induced cellular projections and subsequent viral spread.

METHODS

Virus and Cells

The Gilden VZV strain, isolated from the zoster vesicle of a 75-year-old man, was propagated in human fetal lung fibroblasts (ATCC, Manassas, VA) and cryopreserved at passage 3. Whole genome–based genotyping identified the strain as a clade 3 isolate (GenBank accession number MH379685).

Primary human spinal astrocytes (HA-sps; ScienCell, Carlsbad, CA) were used; cell type was confirmed by an immunofluorescence antibody assay (IFA), using an anti-GFAP antibody and 4′,6-diamidino-2-phenylindole (DAPI) nuclear DNA stain, and cells were quantitated by Fiji image processing software (available at: https://fiji.sc/).

Cell-associated infections were used in all experiments to more accurately represent infection in vivo. HA-sps were seeded at a volume of 5000 cells/cm^2 in basal astrocyte medium containing 2% fetal bovine serum, 1% astrocyte growth supplement, and 1% 100× penicillin-streptomycin (ScienCell). After 24 hours, medium was changed to basal astrocyte medium containing 0.1% fetal bovine serum and 1% 100× penicillin-streptomycin and was replenished every 72 hours for 7 days, establishing quiescence. On day 7, quiescent HA-sps (qHA-sps) were exposed to lysed, VZV-infected human fetal lung fibroblasts; medium was changed at 24 hours, and qHA-sps were harvested 3 days after infection and cryopreserved as a stock for cell-associated infections. Samples were thawed, and VZV was quantified by titration to 100 plaque-forming units/μL and verified for the absence of mycoplasma. Quiescent HA-sps were cocultivated with either VZV-infected HA-sps (0.008 multiplicity of infection [MOI]) or uninfected (ie, mock-infected) HA-sps and analyzed 3 days after infection, when individual VZV-infected cells were still clearly visualized adjacent to uninfected cells (<30% infected cells/culture).

To determine the contribution of replicating virus in NK-1R signaling, VZV lysates that were and those that were not exposed to UV irradiation, to inactivate infectious virus, were used. VZV-infected HA-sps were lysed and exposed to UV or ambient light for 1 hour, added to uninfected qHA-sps at a MOI of 0.008, and analyzed 3 days after infection by IFA.

Flow Cytometry

To determine the extent of VZV infection 3 days after infection, mock- and VZV-infected qHA-sps were harvested and analyzed for expression of VZV glycoprotein E (gE; Millipore, Billerica, MA), using flow cytometry as described elsewhere [25].

Substance P (subP) Enzyme-Linked Immunosorbent Assay (ELISA)

At day 3 after infection, supernatant from mock- and VZV-infected qHA-sps were analyzed for subP, using a colorimetric competitive ELISA per the manufacturer's instructions (Enzo, Farmingdale, NY). Rhesus macaque serum normally containing subP served as positive control [26].

IFA

Quiescent HA-sps were cultured with cell-associated virus, uninfected cells, and VZV lysate, with or without UV treatment, in 24-well μ-plates (ibidi, Martinsried, Germany). Three days after infection, qHA-sps were fixed with 4% paraformaldehyde, permeabilized in 0.3% Triton X-100 for 20 minutes (GFAP) or 0.15% Triton X-100 for 10 minutes (NK-1R), blocked in 10% normal donkey serum (Jackson ImmunoResearch, West Grove, PA) for 1 hour, and stained with a 1:500 dilution of either mouse anti-human VZV gE (Santa Cruz Biotechnology, Santa Cruz, CA) or mouse anti-human VZV glycoprotein B (gB; Abcam, Cambridge, MA). GFAP and NK-1R were detected using chicken anti-GFAP (1:500 dilution; Abcam) and polyclonal rabbit anti-NK-1R (1:100 dilution; Novus Biologicals, Littleton, CO) directed against the N-terminus, respectively. Primary antibodies were incubated overnight at 4°C. Secondary antibodies consisted of Alexa Fluor 488 donkey anti-rabbit immunoglobulin G (IgG; Invitrogen, Carlsbad), 594 donkey anti-mouse IgG (Invitrogen), and 647 donkey anti-chicken IgG (MilliporeSigma, Burlington, MA), all at a dilution of 1:500 for 1 hour at room temperature. After secondary antibody application and phosphate-buffered saline washes, DAPI (Vector Laboratories, Burlingame, California) was added at 1:500 for 5 minutes, washed 3 times, and stored in 2 mL of phosphate-buffered saline. Cells were visualized by confocal microscopy (using a 3I Marianas inverted spinning disk on Zeiss Axio observer Z1; Oberkochen, Germany) and analyzed using 3I Slidebook 6 software.

As a control to verify NK-1R localization when bound to the endogenous ligand, subP, uninfected qHA-sps were treated with 10^{-6} M subP (Abcam) for 60 minutes and visualized for process

formation with CellTracker Deep Red (Invitrogen) or fixed and examined for the distribution of NK-1R by IFA.

Calcium Imaging

To determine whether the subP-NK-1R signaling pathway was intact in HA-sps as shown by calcium flux, qHA-sps were incubated for 30 minutes with 2 μM Fluo-4 AM (Invitrogen) fluorescent calcium indicator diluted in imaging solution (125 mM NaCl, 5.7 mM KCl, 2.5 mM $CaCl_2$, 1.2 mM $MgCl_2$, 10 mM HEPES, pH 7.4) and treated with 10^{-6} M subP (Abcam). Cells were imaged live using a Zeiss LSM 800 microscope before and after subP treatment; calcium flux was quantitated using Fiji software.

Treatment With the NK-1R Antagonists Aprepitant and Rolapitant

Twelve hours after infection, VZV-infected HA-sps were treated with 10 μM aprepitant (Selleckchem, Houston, TX), 5 μM rolapitant (AdooQ, Irvine, CA; optimal concentrations without cell toxicity were determined in preliminary assays on uninfected qHA-sps, using 1–100 μM aprepitant and 1–50 μM rolapitant; data not shown), or vehicle (DMSO) and retreated at 24 and 48 hours after infection. Light microscopy images were obtained 12, 24, 48, and 72 hours after infection, followed by DNA extraction and quantitative polymerase chain reaction (qPCR) for VZV DNA.

DNA/RNA Extraction and qPCR

DNA was extracted using the DNeasy Blood and Tissue Kit (Qiagen, Germantown, MD); RNA was extracted using the Direct-zol RNA MiniPrep kit (Zymo Research, Irvine) and reverse transcribed using the Transcriptor High Fidelity cDNA Synthesis Kit (Roche, Basel, Switzerland). DNA and complementary DNA were analyzed with qPCR primers corresponding to VZV open reading frame 68 and glyceraldehyde-3-phosphate-dehydrogenase (GAPdH) as described elsewhere [27], as well as primers specific for all NK-1R isoforms (spanning exon 1, since truncations occur at the 3′ end and all isoforms contain exon 1) and full-length-only NK-1R isoforms (spanning exon 5; prevalidated primers Hs.PT.58.28023671.g and Hs.PT.58.40639132.g; Integrated DNA Technologies, Coralville, IA). Data were normalized to GAPdH and analyzed using the ΔΔ threshold cycle method.

Western Blot Analysis

At 3 days after infection, cell membrane/cytoplasmic and nuclear protein fractions from mock- and VZV-infected qHA-sps were isolated by a micropreparation technique [28] and 30 μg/fraction analyzed by western blot as previously described [29]. Polyvinylidene difluoride membranes were probed using a polyclonal rabbit anti-NK-1R antibody (1:100 dilution; Novus Biologicals) diluted in blocking solution (1× casein) overnight at 4°C. Secondary goat anti-rabbit IgG antibody conjugated to horseradish peroxidase (Abcam) was diluted 1:1000 and incubated at room temperature for 1 hour. Reactions were examined using the SuperSignal West Femto Maximum Sensitivity Substrate (ThermoFisher Scientific, Waltham, MA). Blots were stripped, blocked for 1 hour, and probed with the control antibodies lamin B1 (1:100 dilution; Cell Signaling Technology, Danvers, MA) and β-actin (1:2000 dilution; Cell Signaling Technology). Western blot products were evaluated in a single image, using the Fiji gel analysis tool.

Statistical Analysis

Statistical analysis was performed using GraphPad Prism (GraphPad, San Diego, CA). Significant differences in VZV DNA levels between treated and untreated VZV-infected qHA-sps at each time point were determined using the unpaired Student *t* test. A 2-tailed binomial test was used to determine statistical significance in cytoplasmic versus nuclear protein expression ratios of NK-1R between groups (expected outcomes were generated from mock-infected qHA-sps).

RESULTS

Primary Human Spinal Astrocytes Are Permissive to VZV Infection and Develop Lamellipodia and Filopodia

All DAPI-positive qHA-sps contained GFAP (total cells counted, 9787), indicating a homogeneous astrocyte culture (Figure 1A). Quiescent HA-sps were permissive to infection, with VZV-gB–positive cells exhibiting cellular projections (ie, lamellipodia) contacting adjacent uninfected cells (Figure 1B). Higher magnification of a VZV-infected qHA-sp (Figure 1C) showed the striking morphology of a lamellipodium, which contained slender cytoskeletal projections (ie, filopodia). In contrast, uninfected qHA-sps adjacent to a VZV-infected qHA-sp with lamellipodia showed a normal polygonal morphology (Figure 1D). Additional images demonstrated the complex structure of lamellipodia in VZV-infected qHA-sps (Supplementary Figure 1*A* and 1*B*).

VZV Infection Is Associated With Nuclear Localization of NK-1R in Primary Human Spinal Astrocytes in the Absence of the Endogenous Ligand, subP

Three days after infection, IFA revealed diffuse NK-1R in the cell membrane/cytoplasm of mock-infected qHA-sps (Figure 2A), with minimal NK-1R detected within the nucleus on z-stack imaging (Figure 2B). In contrast, a VZV-gE-positive qHA-sp (Figure 2C) contained NK-1R predominantly in the nucleus (Figure 2C and 2D), as confirmed by z-stack imaging. Quiescent HA-sps during early infection were identified at the borders of VZV-infected cell clusters. A qHA-sp during early infection was identified by the presence of a small amount of VZV gB along the bottom of the nucleus (Figure 2E) and the onset of adjacent NK-1R nuclear localization. Experiments using VZV lysates without or with UV irradiation revealed similar findings; qHA-sps exposed to VZV lysates contained VZV-gB–positive cells with nuclear NK-1R, while qHA-sps

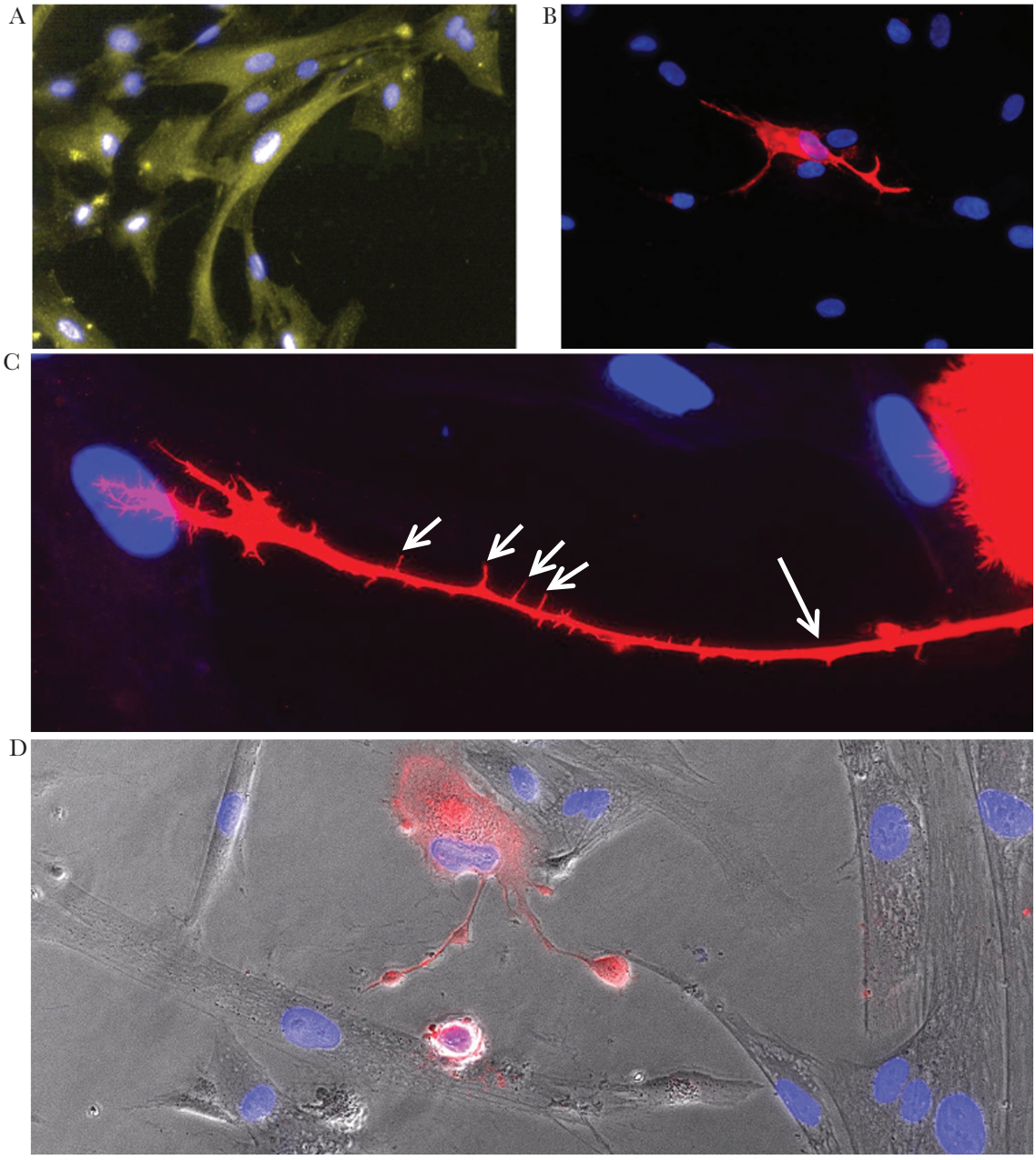

Figure 1. Infection of primary human spinal astrocytes with varicella zoster virus (VZV). Quiescent primary human spinal astrocytes (qHA-sps) were mock- or VZV-infected and analyzed by immunofluorescence antibody assay 3 days after infection, using antibodies against glial fibrillary acidic protein (GFAP; an astrocyte marker) or VZV glycoprotein B (gB). GFAP was seen in all cells (yellow; *A*), confirming a pure astrocyte culture. Quiescent HA-sps were permissive to VZV infection, as shown by a cell expressing VZV gB (red; *B*); note the projections (lamellipodia) of the infected cell extending to surrounding uninfected cells. A higher-magnification image of a VZV-infected astrocyte (red; *C*) showed a strikingly long lamellipodium (long arrow) that extends toward an uninfected cell; filopodia (short arrows) were also seen sprouting from the lamellipodium. A phase-contrast image overlay demonstrated the normal morphology of uninfected bystander HA-sps (clear cells) and 2 lamellipodia arising from a VZV-infected astrocyte (red cell; *D*). Blue indicates cell nuclei. Original magnification ×400 (*A, B,* and *D)* and ×600 (*C*).

exposed to UV-irradiated lysates expressed no VZV gB or nuclear NK-1R (Supplementary Figure 2).

ELISA of positive control rhesus macaque serum revealed 5652 pg/mL of subP, whereas supernatant from mock- and VZV-infected HA-sps had no detectable subP (assay range, 9.76–10 000 pg/mL), indicating that VZV-induced nuclear localization of NK-1R is subP independent.

VZV Infection Is Associated With Nuclear Localization of 3 NK-1R Isoforms

Three days after infection, flow cytometry confirmed that only 20% of cells were infected (Figure 3A), demonstrating that VZV cultures were not overly infected and contained dying cells with disrupted nuclear membranes that may interfere with accurate nuclear localization of NK-1R. Western blot demonstrated

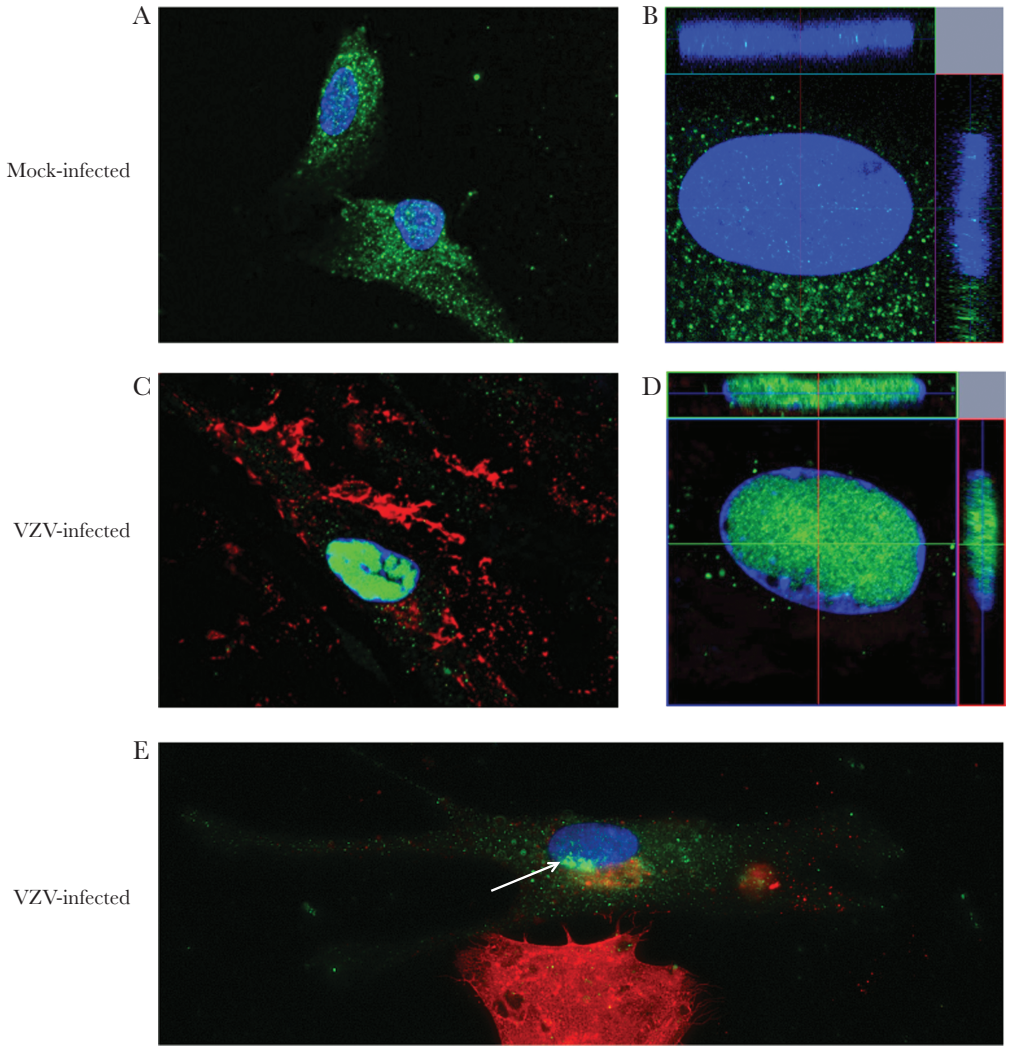

Figure 2. Neurokinin-1 receptor localization in mock- and varicella zoster virus (VZV)–infected primary human spinal astrocytes, detected by immunofluorescence antibody assay (IFA). Quiescent primary human spinal astrocytes were mock- or VZV-infected and analyzed by IFA 3 days after infection, using an antibody against neurokinin-1 receptor (NK-1R) and VZV glycoprotein E (gE) or B (gB). NK-1R was expressed predominantly in the cytoplasm of mock-infected cells (green; *A*) and to a much lesser extent in the nucleus, as shown in a z-stack image (green; *B*). In an infected cell expressing VZV gE (red; *C*), NK-1R was expressed predominantly in the nucleus (green; *C*) and to a much lesser extent in the cytoplasm, as shown by a z-stack image (green; *D*). An astrocyte during early infection (top cell; *E*) showed only minimal VZV gB (red) in the cytoplasm at the bottom edge of the nucleus as compared to the intense VZV gB (red) throughout a highly infected cell on the bottom of the panel. In the early infected cell, NK-1R appeared to begin localizing to the nucleus adjacent to VZV gB (green [white arrow]; *E*). Original magnification ×400 (*A, C,* and *E*) and ×600 (*B* and *D*).

a distinct lamin band (66 kDa) in nuclear but not cell membrane/cytoplasmic fractions. Use of a polyclonal anti–NK-1R antibody to confirm IFA results and determine the NK-1R isoforms involved revealed the expression of 3 NK-1R isoforms (a 46-kDa full-length isoform and 38- and 33-kDa truncated isoforms) in qHA-sps (Figure 3B). The 38-kDa isoform was present predominantly in the cell membrane/cytoplasm of VZV- and mock-infected cells (Figure 3B) and predominantly in the nucleus of VZV-infected cells, but it was not detected in the nucleus of mock-infected cells. Since this band was not as intense as those of the other 2 isoforms, it is possible that a small amount of the 38-kDa isoform was present in cell membrane/cytoplasm but not detected with the amount of protein loaded; however, there remained a significant shift of this isoform to the nucleus during VZV infection. In contrast, both nuclear and cell membrane/cytoplasmic fractions of VZV- and mock-infected lysates contained the full-length and truncated 33-kDA isoforms (Figure 3B); however, during VZV infection, there was a significant shift of these 2 isoforms into the nucleus. Calculation of band intensities by using the Fiji gel analysis tool showed that percentages of cytoplasmic and nuclear full-length NK-1R expression in mock-infected qHA-sps (70.6% and 29.4%, respectively) shifted following VZV infection (59.3% and 40.7%, respectively; $P < .05$, by the 2-tailed binomial test; Figure 3C; left panel). The 33-kDa isoform showed a similar shift in mock-infected qHA-sps (77.8% and 22.2%, respectively)

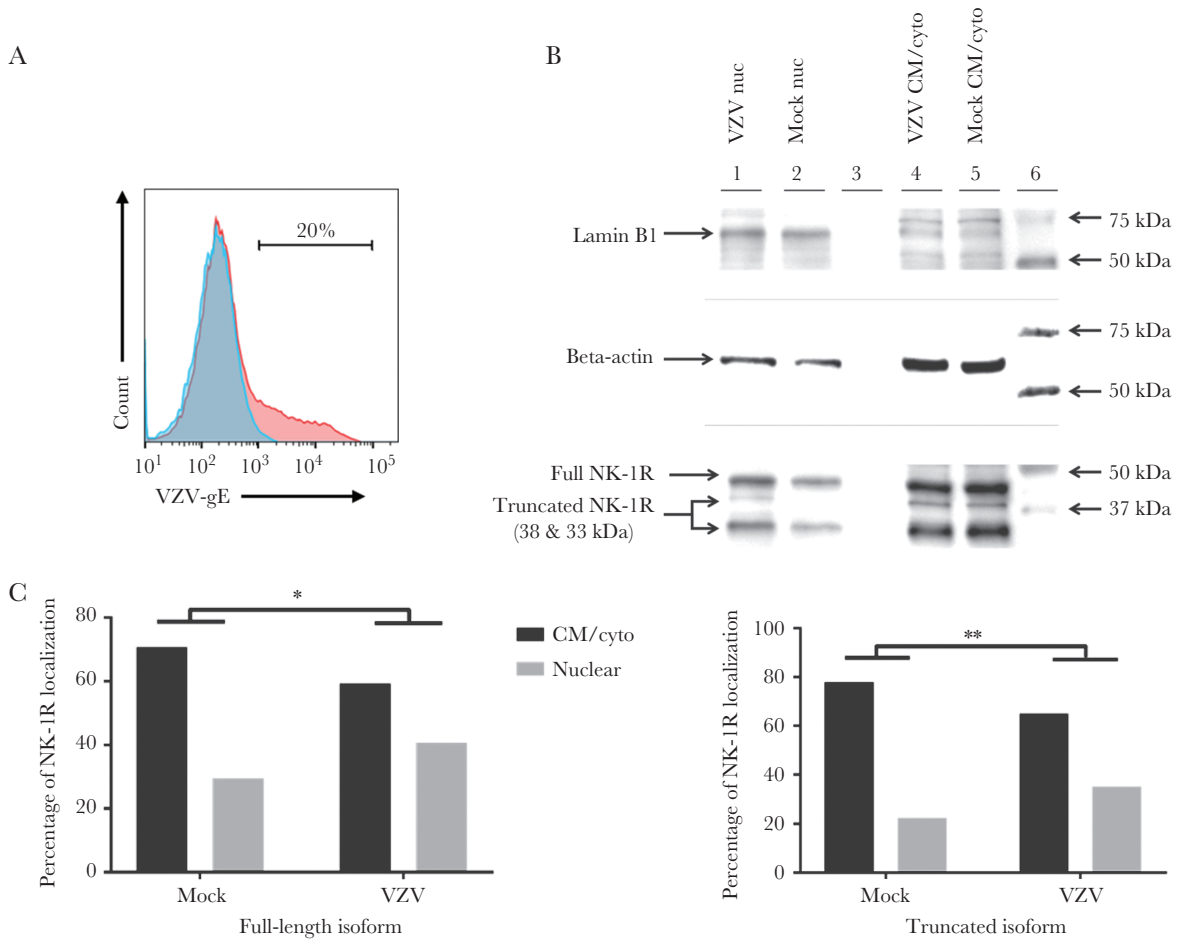

Figure 3. Neurokinin-1 receptor localization in mock- and varicella zoster virus (VZV)–infected primary human spinal astrocytes, determined by Western blot. Quiescent primary human spinal astrocytes (qHA-sps) were mock- or VZV-infected and analyzed for VZV glycoprotein E (gE) expression, using flow cytometry; mock-infected cells did not contain VZV gE (blue; *A*), whereas 20% of cells in VZV-infected cultures expressed VZV gE (red; *A*). These early infection cultures were used for Western blot to eliminate the potential of virus-induced cell death at high infection rates that may disrupt the integrity of the nuclear membrane and accurate quantitation of nuclear neurkinin-1 receptor (NK-1R) localization. Nuclear (nuc) and cell membrane/cytoplasmic (CM/cyto) fractions prepared from mock- and VZV-infected qHA-sps 3 days after infection revealed 3 isoforms of NK-1R: the full-length isoform, at 46 kDa, and 2 truncated isoforms, at approximately 38 and 33 kDa. The 38-kDa NK-1R isoform was present only in the CM/cyto of both VZV- and mock-infected cells (lanes 4 and 5; *B*) but shifted predominantly to the nucleus during VZV infection (lane 1; *B*); no nuclear shift was seen in mock-infected HA-sps (lane 2; *B*). In contrast, both nuc and CM/cyto fractions of VZV- and mock-infected lysates contained the full-length and truncated 33-kDa NK-1R isoforms (lanes 1, 2, 4, and 5; *B*); however, during VZV infection, a fraction of these isoforms appeared to shift to the nucleus, compared with observations during mock infection. Band intensities calculated using the Fiji gel analysis tool indicated that, in mock-infected cells, 70.6% of full-length NK-1R was located in the CM/cyto and 29.4% in the nuc fractions, compared with 59.3% in CM/cyto and 40.7% in nuc fractions of VZV-infected HA-sps (left panel; *C*). Comparison of the proportions of nuclear full-length NK-1R to total NK-1R showed a significant increase in nuclear NK-1R in VZV-infected cells, compared with mock-infected cells (*$P < .05$). Similarly, quantitation of band intensities of the 33-kDa NK-1R isoform showed that, in mock-infected cells, 77.8% of NK-1R was located in the CM/cyto and 22.2% in the nuc fractions, compared with 64.9% in CM/cyto and 35.1% in nuc fractions of VZV-infected HA-sps (right panel; *C*); comparison of the proportions of nuclear 33-kDa NK-1R to total 33-kDa NK-1R showed a significant increase in nuclear 33-kDa NK-1R in VZV-infected cells as compared to mock-infected cells (**$P < .01$). Of note, these proportions of nuclear NK-1R localizing to the nucleus during infection were underestimates, since the VZV-infected cultures contained approximately 80% uninfected bystander cells with predominantly cytoplasmic NK-1R.

versus VZV-infected qHA-sps (64.9% and 35.1%, respectively; $P < .01$, by the 2-tailed binomial test; Figure 3C; right panel). Of note, the percentages of NK-1R localizing to the nucleus during infection were an underestimate because the VZV-infected cultures contained approximately 80% uninfected bystander cells with predominantly cell membrane/cytoplasmic NK-1R.

PCR amplification of NK-1R revealed more amplified product from primers that detected all isoforms than from primers that detected only the full-length isoform (mean ΔCt [±SD], 11.59 ± 0.11 vs 13.22 ± 0.09; n = 3), suggesting that RNA from truncated isoforms was also contributing to total amplified products. There was not a notable change in full-length or all NK-1R transcripts during VZV infection.

subP Does Not Induce Nuclear Localization of NK-1R or Formation of Lamellipodia

Uninfected qHA-sps treated with subP expressed NK-1R predominantly in the cell membrane/cytoplasm (Supplementary Figure 3*A* and 3*B*), unlike the nuclear localization of NK-1R in VZV-infected qHA-sps (Figure 2C and 2D). No lamellipodia

in subP-treated qHA-sps were detected by staining with CellTracker Deep Red (Supplementary Figure 3*C*). Calcium imaging of qHA-sps before and after subP treatment demonstrated an increase in calcium flux, confirming functional NK-1R in the astrocytes (Supplementary Figure 3*D*–*F*).

NK-1R Antagonists Aprepitant and Rolapitant Block Formation of Lamellipodia and Reduce Viral DNA and Spread in VZV-Infected Spinal Astrocytes

Three days after infection, VZV-infected qHA-sps (Figure 4A and 4B) treated with vehicle revealed lamellipodia and predominantly nuclear NK-1R, while uninfected bystander cells showed neither lamellipodia nor nuclear NK-1R. VZV-infected qHA-sps treated with 10 μM aprepitant showed reduced formation of lamellipodia but retention of nuclear NK-1R in some cells (Figure 4C and 4D). In complimentary experiments, once VZV infection was established 12 hours after infection, qHA-sps were treated with vehicle or 10 μM aprepitant; drug was reapplied 24 and 48 hours after infection (Figure 5A). At 12, 24, 48 and 72 hours after infection, qHA-sps were visualized by light microscopy, and DNA was harvested and analyzed by qPCR. Forty-eight hours after infection, vehicle-treated qHA-sps had significantly higher amounts of VZV DNA than aprepitant-treated qHA-sps, compared with amounts 12 hours after infection (mean fold-increase [±SD], 121 ± 29.2 vs 10.5 ± 3.8; $P < .01$; n = 3); similar results were seen 72 hours after infection (mean fold-increase [±SD], 452.9 ± 122.9 vs 24.9 ± 6.9; $P < .01$; n = 3; Figure 5B). Thus, aprepitant treatment reduced VZV DNA levels by a mean (±SD) of 91% ± 0.03% and 94% ± 0.01% 48 and 72 hours after infection, respectively. Light microscopy demonstrated a cytopathic effect 48 and 72 hours after infection in VZV-infected/vehicle-only samples (Figure 5C) but not in aprepitant-treated samples.

In parallel experiments, application of the NK-1R antagonist rolapitant (5 μM) also reduced the cytopathic effect in VZV-infected qHA-sps as compared to mock-infected qHA-sps 48 and 72 hours after infection (Figure 6A). In VZV-infected qHA-sps, rolapitant reduced lamellipodia formation (Figure 6B), similar to aprepitant treatment (Figure 4A–D). The mean VZV DNA level (±SD) was significantly reduced 48 and 72 hours after infection (by 94% ± 0.003% and 96% ± 0.01%, respectively; $P < .001$; n = 3) following rolapitant treatment, compared with VZV-infected/vehicle-only samples (Figure 6C).

DISCUSSION

Herein, we found that VZV infection of human spinal astrocytes is associated with nuclear localization of NK-1R and lamellipodia/filopodia formation that may facilitate cell-to-cell spread of VZV (Figure 7). Additionally, 2 NK-1R antagonists

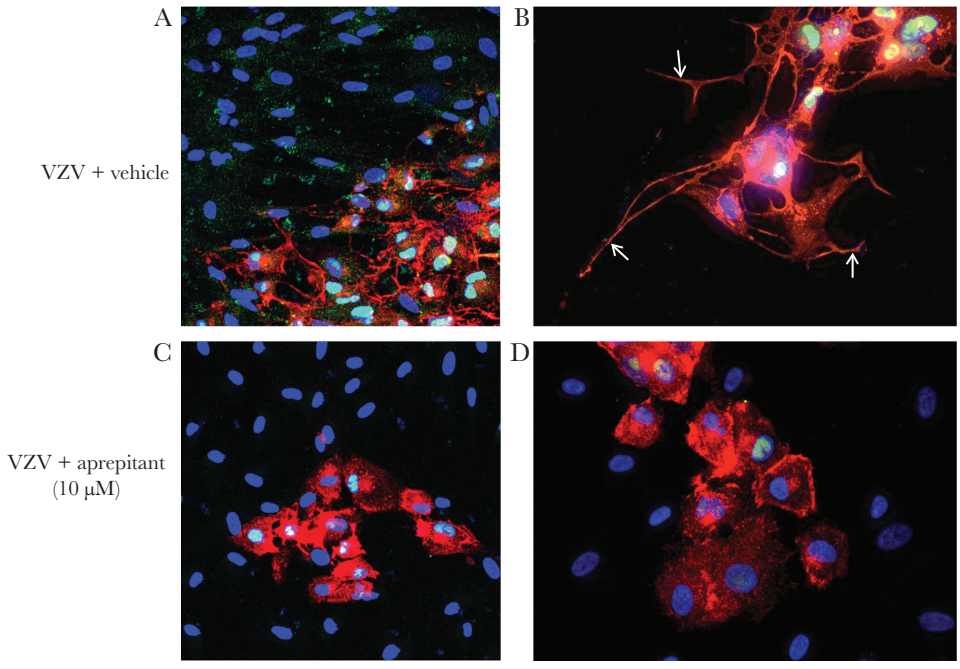

Figure 4. Treatment of varicella zoster virus (VZV)–infected primary human spinal astrocytes (HA-sps) with aprepitant, a neurokinin-1 receptor antagonist. Quiescent HA-sps (qHA-sps) were infected with VZV in the presence of vehicle (dimethyl sulfoxide) with or without 10 μM aprepitant and analyzed by immunofluorescence antibody assay 3 days after infection, using an antibody against neurokinin-1 receptor (NK-1R) and VZV glycoprotein B (gB). VZV-infected HA-sps expressing VZV gB (red) had long, extended processes (lamellipodia) and predominantly nuclear localization of NK-1R (green; *A*), while uninfected bystander cells did not have nuclear NK-1R. High magnification showed a network of lamellipodia extending from cell bodies of VZV-infected qHA-sps (*B*, arrows); note the nuclear localization of NK-1R (green). Application of the NK-1R antagonist aprepitant reduced the extension of lamellipodia in infected cells expressing VZV gB (red; *C*), with fewer cells containing nuclear NK-1R (green). High magnification demonstrated a clear reduction in lamellipodia of VZV-infected qHA-sps treated with aprepitant (red; *D*). Original magnification ×200 (*A* and *C*) and ×400 (*B* and *D*).

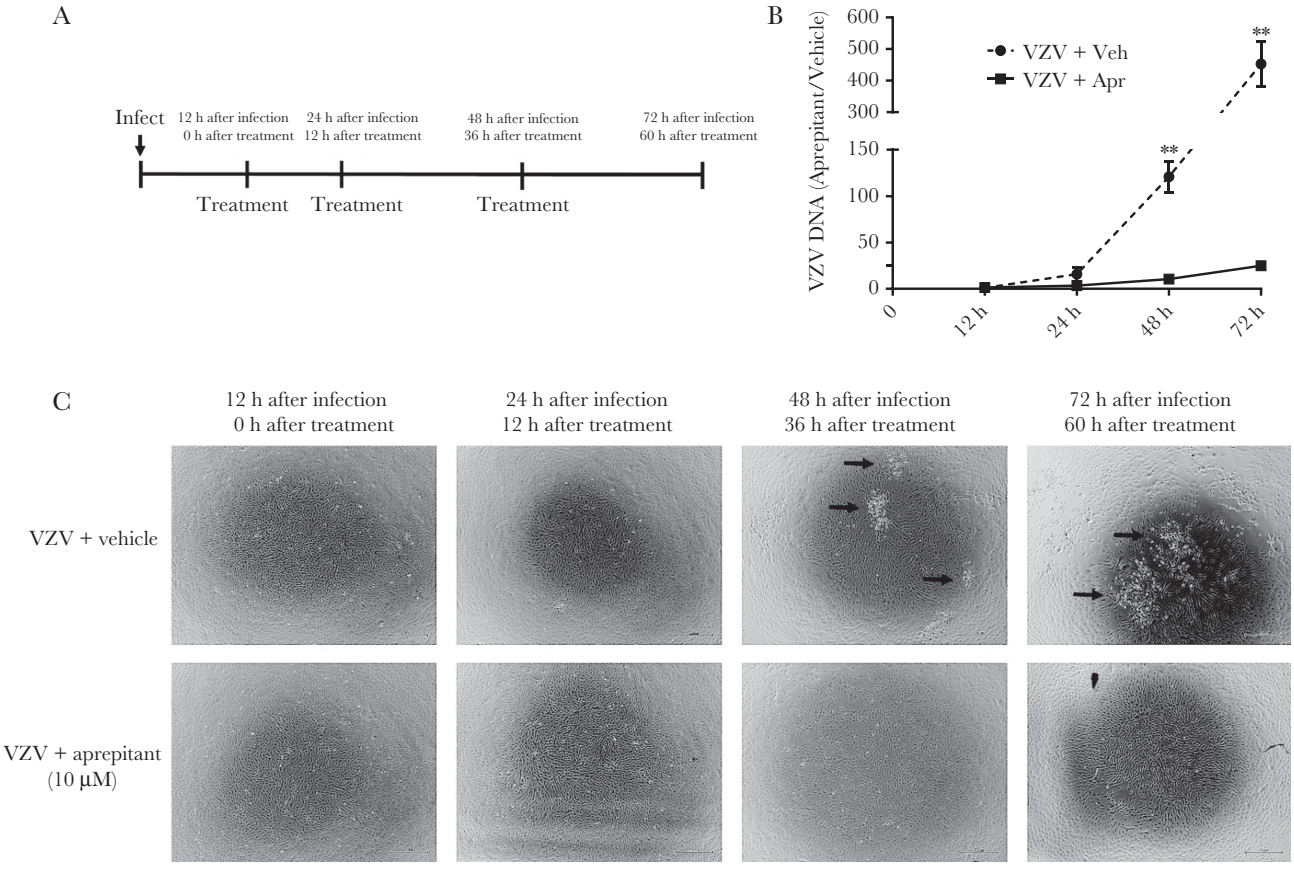

Figure 5. Reduction in varicella zoster virus (VZV) DNA level and viral spread after treatment with the neurokinin-1 receptor antagonist aprepitant. Quiescent primary human spinal astrocytes (qHA-sps) were infected with VZV; 12 hours after infection, qHA-sps were treated with vehicle (dimethyl sulfoxide) or with 10 μM aprepitant. Treatment was reapplied 24 and 48 hours after infection (*A*). At 12, 24, 48, and 72 hours after infection (corresponding to 0, 12, 36, and 60 hours after treatment, respectively), qHA-sps were visualized by light microscopy in vehicle- and aprepitant-treated cultures and harvested for DNA. At 48 hours after infection, vehicle-treated qHA-sps had significantly higher amounts of VZV DNA than aprepitant-treated qHA-sps, compared with findings 12 hours after infection (mean fold-increase [±SD], 121 ± 29.2 vs 10.5 ± 3.8; $P < .01$; n = 3); similar results were seen 72 hours after infection (452.9 ± 122.9 vs 24.9 ± 6.9; $P < .01$; n = 3; *B*). The *y*-axis represents the fold change of VZV-infected qHA-sps treated with vehicle only (dotted line; n = 3) or aprepitant (solid line; n = 3), compared with findings 12 hours after infection, before treatment. Thus, aprepitant treatment reduced the VZV DNA level by a mean percentage (±SD) of 91% ± 0.03% and 94% ± 0.01% at 48 and 72 hours after infection, respectively. Corresponding light microscopy images demonstrated a cytopathic effect 48 and 72 hours after infection (corresponding to 36 and 60 after treatment, respectively) in VZV-infected, vehicle-only samples (arrows in upper panels; *C*) but not in aprepitant-treated samples (lower panels; *C*).

(aprepitant and rolapitant), already in clinical use as antiemetics, prevent formation of lamellipodia and inhibit viral spread, providing novel antiviral treatments for VZV infection. Several important points emerged from these studies.

While outgrowth of lamellipodia occurs during astrocyte activation and gliosis in response to CNS injury [30–33], NK-1R–dependent/VZV-induced HA-sp lamellipodia were not diffusely spread but rather appeared to migrate preferentially toward uninfected cells. This unusual morphology and nuclear localization of NK-1R in the absence of subP was not seen in uninfected bystander cells or cells exposed to UV-irradiated VZV lysates, indicating that productive virus infection was required. This morphology and NK-1R nuclear localization was also not seen in uninfected qHA-sps treated with subP. Furthermore, the expected reactive gliosis of surrounding uninfected qHA-sps exposed to VZV-infected cells, cytokines, and other soluble factors that were presumably released did not occur, with no signs of activation and with normal maintenance of their polygonal shapes in vitro. This suggested that the "danger" signals to prime surrounding astrocyte reactivity were not present or functional. The induction of extensive lamellipodia and filopodia in VZV-infected qHA-sps was most likely involved in cell-to-cell spread of VZV, consistent with a study showing that, during VZV infection of human melanoma cells, VZV particles emerged on the cell surface amid actin-based filopodia, which were abundant within viral highways [22].

Typically, NK-1R is expressed on the cell surface, and when subP binds, the ligand-receptor complex is internalized to endosomes within cytoplasm [34], ultimately modulating multiple cellular processes, including pain transmission, neuroimmune modulation, and vasodilation. Subsequently, the complex dissociates, subP is degraded, and NK-1R is reexpressed on the cell

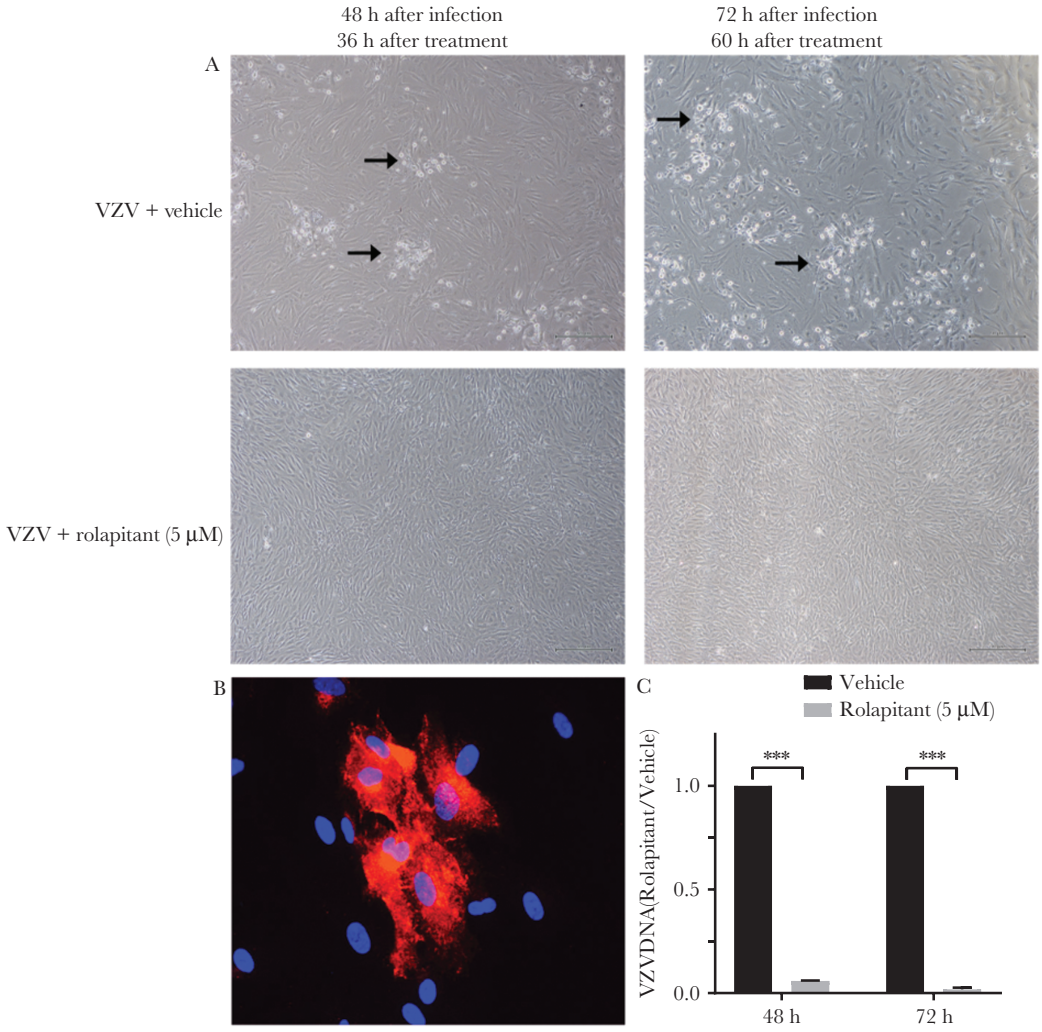

Figure 6. Reduction in varicella zoster virus (VZV) DNA and viral spread after treatment with the neurokinin-1 receptor antagonist rolapitant. Quiescent primary human spinal astrocytes (qHA-sps) were infected with VZV and, after 12 hours, were treated with vehicle (dimethyl sulfoxide) or with 5 μM rolapitant. Treatment was reapplied 24 and 48 hours after infection. Light microscopy images demonstrated the formation of a cytopathic effect 48 and 72 hours after infection (corresponding to 36 and 60 hours after treatment, respectively) in vehicle-treated VZV-infected cells (arrows in upper panels; *A*) but not in rolapitant-treated cells (lower panels; *A*). At 72 hours after infection, qHA-sps analyzed by immunofluorescence antibody assay, using an antibody against VZV glycoprotein B (red; *B*), showed no cellular projections. Compared with vehicle-treated, VZV-infected cells, rolapitant-treated, VZV-infected cells had significantly lower amounts of VZV DNA 48 hours after infection (mean reduction [±SD], 94% ± 0.003% reduction; ***P < .001; n = 3) and 72 hours after infection (96% ± 0.01%; ***P < .001; n = 3), as quantified by quantitative polymerase chain reaction analysis (*C*). Original magnification ×400 (*B*).

surface. During early VZV infection, NK-1R begins to accumulate in the nucleus in an asymmetrical manner in association with VZV gB; during late infection, when VZV gB is found diffusely in the cell, NK-1R is predominantly nuclear. Since subP was not detected in VZV-HA-sps, the redistribution of NK-1R and subsequent formation of lamellipodia may be induced by a subP-like molecule. Specifically, VZV gB shares significant sequence homology to the active binding site of subP, although its ability to bind NK-1R remains to be determined. Precedence for binding of a viral protein to NK-1R is shown by measles virus envelope fusion protein and bovine respiratory syncytial virus virokinin binding to NK-1R that facilitates entry to neurons and modulates the host immune response, respectively [19, 20]. Interestingly, studies involving NK-1R–deficient mice showed accelerated development of herpes stromal keratitis following herpes simplex virus type 1 (HSV1) ocular infection [35] and enhanced viral production in the genital tract of HSV2-infected animals [36]. The opposing proviral role of NK-1R during VZV infection may reflect differences in host species, cell types, or viruses. In the HSV studies, deficiency of NK-1R on immune cells may inhibit immune cell activation by subP and interfere with immune-mediated HSV1/2 clearance. Furthermore, since HSV1/2 does not typically spread cell to cell via lamellipodia, it may not exploit NK-1R in the same manner as VZV in HA-sps.

Two NK-1R isoforms have been described in humans, 1 full length and 1 truncated (molecular weight, 46 and 38 kDa,

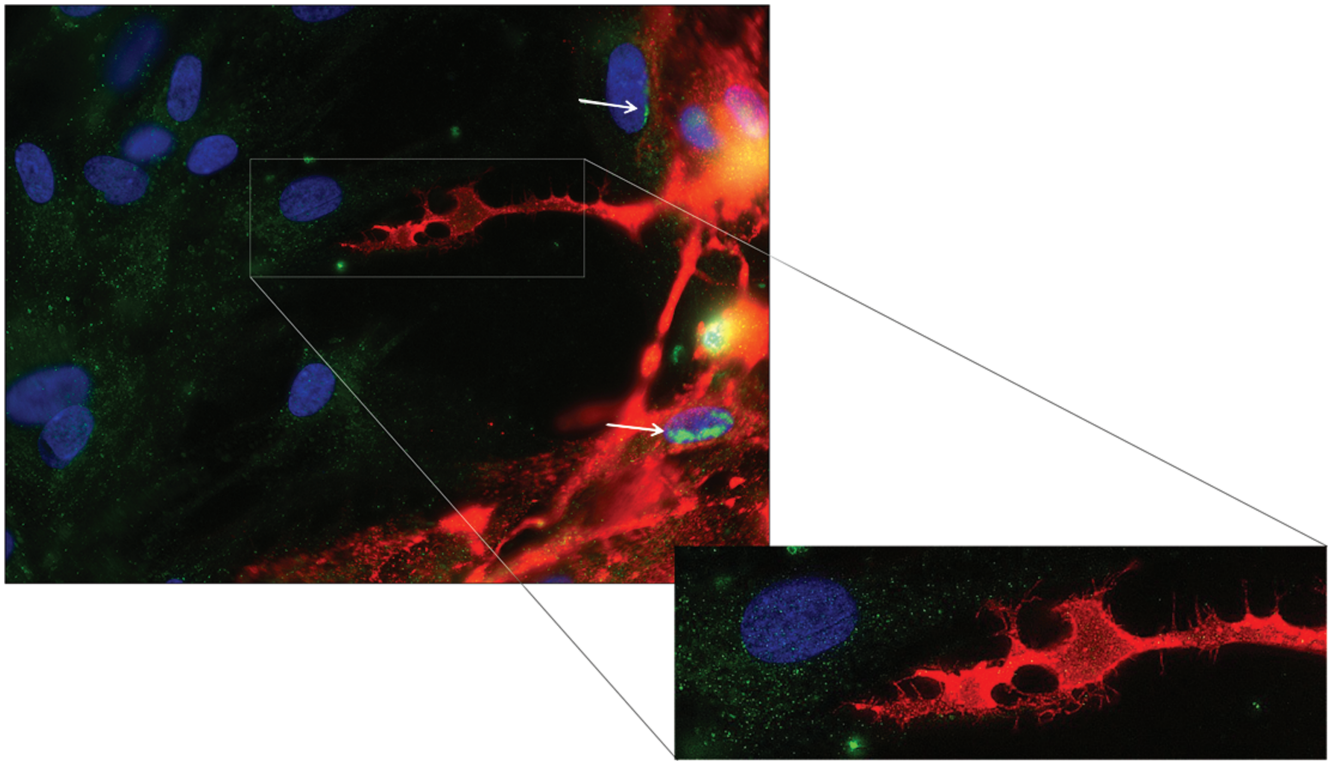

Figure 7. Predominantly nuclear localization of neurokinin-1 receptor in varicella zoster virus (VZV)–infected primary human spinal astrocytes and cytoplasmic localization in uninfected bystander cells. Three days after infection, infected quiescent primary human spinal astrocytes (qHA-sps) expressing VZV glycoprotein B (gB; red) showed neurokinin-1 receptor (NK-1R) predominantly in the nucleus (green-yellow) and aberrant lamellipodia. Uninfected bystander cells had predominantly cytoplasmic, diffuse NK-1R (green) without VZV gB. Early infection, demonstrated by cells along the infected edge (upper right), showed the start of NK-1R nuclear migration (green [arrows]). Blue indicates nuclei. Original magnification ×400.

respectively); however, multiple isoforms have been reported in human cancer cells, including a 33-kDa isoform [37–41]. Herein, we found 3 distinct isoforms in HA-sps: 46- and 33-kDa isoforms that were present in both the cell membrane/cytoplasm and nucleus but increased in the nucleus during VZV infection and a 38-kDa isoform that was predominantly in the cell membrane/cytoplasm and shifted almost completely to the nucleus during VZV infection. The presence of 3 NK-1R isoforms in HA-sps differs from a study that found only the full-length isoform in nonhuman primate frontal cortex brain slices and in an immortalized human astrocytic cell line [42]. Our findings of multiple isoforms in HA-sps raises the intriguing possibility of region-specific differences in astrocytes, since prior studies used cortical astrocytes, whereas our studies used spinal cord astrocytes, which have not been characterized for NK-1R isoforms. Finally, reports of nuclear localization of NK-1R are rare, with most involving cancer cells and human adipose tissue stem cells [39, 43], and the physiological significance of this localization remains unclear, although involvement in transcriptional alterations has been speculated [43]. In our case, nuclear NK-1R appears to be associated with distinct phenotypic alterations promoting viral spread.

Overall, we have demonstrated the proviral role of NK-1R in VZV infection and identified promising new antiviral drugs, aprepitant and rolapitant. VZV infection in HA-sps provides a useful model to elucidate additional mechanisms involved in VZV myelopathy.

Supplementary Data

Supplementary materials are available at *The Journal of Infectious Diseases* online. Consisting of data provided by the authors to benefit the reader, the posted materials are not copyedited and are the sole responsibility of the authors, so questions or comments should be addressed to the corresponding author.

Notes

Acknowledgments. We thank Marina Hoffman, for editorial review; Cathy Allen, for manuscript preparation; and Dr Ravi Mahalingam, Department of Neurology, University of Colorado School of Medicine, for contribution of rhesus macaque control serum.

Financial support. This work was supported by the National Institutes of Health (grant AG032958, to M. A. N. and R. J. C.; grant NS094758, to M. A. N.; grant NS082228, to R. J. C.; grant NS093716, to N. L. B.; and grants R21AI121528 and R21CA209229, to S. F.) and the American Cancer Society (institutional research grant 14-196-01 to S. F.).

Potential conflicts of interest. All authors: No reported conflicts. All authors have submitted the ICMJE Form for Disclosure of Potential Conflicts of Interest. Conflicts that the editors consider relevant to the content of the manuscript have been disclosed.

References

1. Kennedy PG, Grinfeld E, Gow JW. Latent varicella-zoster virus is located predominantly in neurons in human trigeminal ganglia. Proc Natl Acad Sci U S A **1998**; 95:4658–62.
2. Kennedy PG, Grinfeld E, Gow JW. Latent Varicella-zoster virus in human dorsal root ganglia. Virology **1999**; 258:451–4.
3. Nagel MA, Rempel A, Huntington J, Kim F, Choe A, Gilden D. Frequency and abundance of alphaherpesvirus DNA in human thoracic sympathetic ganglia. J Virol **2014**; 88:8189–92.
4. Gilden DH, Beinlich BR, Rubinstien EM, et al. Varicella-zoster virus myelitis: an expanding spectrum. Neurology **1994**; 44:1818–23.
5. Manian FA, Kindred M, Fulling KH. Chronic varicella-zoster virus myelitis without cutaneous eruption in a patient with AIDS: report of a fatal case. Clin Infect Dis **1995**; 21:986–8.
6. Chang CC, McLean C, Vujovic O, et al. Fatal acute varicella-zoster virus hemorrhagic meningomyelitis with necrotizing vasculitis in an HIV-infected patient. Clin Infect Dis **2009**; 48:372–3.
7. Devinsky O, Cho ES, Petito CK, Price RW. Herpes zoster myelitis. Brain **1991**; 114(Pt 3):1181–96.
8. de Silva SM, Mark AS, Gilden DH, et al. Zoster myelitis: improvement with antiviral therapy in two cases. Neurology **1996**; 47:929–31.
9. Lionnet F, Pulik M, Genet P, et al. Myelitis due to varicella-zoster virus in two patients with AIDS: successful treatment with acyclovir. Clin Infect Dis **1996**; 22:138–40.
10. Cuello JP, Romero J, de Ory F, de Andres C. Longitudinally extensive varicella-zoster virus myelitis in a patient with multiple sclerosis. Spine (Phila Pa 1976) **2013**; 38:E1282–4.
11. Yeung J, Cauquil C, Saliou G, et al. Varicella-zoster virus acute myelitis in a patient with MS treated with natalizumab. Neurology **2013**; 80:1812–3.
12. Colombo E, Farina C. Astrocytes: key regulators of neuroinflammation. Trends Immunol **2016**; 37:608–20.
13. Horten B, Price RW, Jimenez D. Multifocal varicella-zoster virus leukoencephalitis temporally remote from herpes zoster. Ann Neurol **1981**; 9:251–66.
14. Moulignier A, Pialoux G, Dega H, Dupont B, Huerre M, Baudrimont M. Brain stem encephalitis due to varicella-zoster virus in a patient with AIDS. Clin Infect Dis **1995**; 20:1378–80.
15. Carpenter JE, Clayton AC, Halling KC, et al. Defensive perimeter in the central nervous system: predominance of astrocytes and astrogliosis during recovery from varicella-zoster virus encephalitis. J Virol **2016**; 90:379–91.
16. Assouline JG, Levin MJ, Major EO, Forghani B, Straus SE, Ostrove JM. Varicella-zoster virus infection of human astrocytes, Schwann cells, and neurons. Virology **1990**; 179:834–44.
17. Kennedy PG, Major EO, Williams RK, Straus SE. Down-regulation of glial fibrillary acidic protein expression during acute lytic varicella-zoster virus infection of cultured human astrocytes. Virology **1994**; 205:558–62.
18. Li Y, Douglas SD, Song L, Sun S, Ho WZ. Substance P enhances HIV-1 replication in latently infected human immune cells. J Neuroimmunol **2001**; 121:67–75.
19. Zimmer G, Rohn M, McGregor GP, Schemann M, Conzelmann KK, Herrler G. Virokinin, a bioactive peptide of the tachykinin family, is released from the fusion protein of bovine respiratory syncytial virus. J Biol Chem **2003**; 278:46854–61.
20. Makhortova NR, Askovich P, Patterson CE, Gechman LA, Gerard NP, Rall GF. Neurokinin-1 enables measles virus trans-synaptic spread in neurons. Virology **2007**; 362:235–44.
21. Meshki J, Douglas SD, Hu M, Leeman SE, Tuluc F. Substance P induces rapid and transient membrane blebbing in U373MG cells in a p21-activated kinase-dependent manner. PLoS One **2011**; 6:e25332.
22. Carpenter JE, Hutchinson JA, Jackson W, Grose C. Egress of light particles among filopodia on the surface of Varicella-Zoster virus-infected cells. J Virol **2008**; 82:2821–35.
23. Douglas SD, Leeman SE. Neurokinin-1 receptor: functional significance in the immune system in reference to selected infections and inflammation. Ann N Y Acad Sci **2011**; 1217:83–95.
24. Greco SJ, Corcoran KE, Cho KJ, Rameshwar P. Tachykinins in the emerging immune system: relevance to bone marrow homeostasis and maintenance of hematopoietic stem cells. Front Biosci **2004**; 9:1782–93.
25. Jones D, Blackmon A, Neff CP, et al. Varicella-zoster virus downregulates programmed death ligand 1 and major histocompatibility complex class I in human brain vascular adventitial fibroblasts, perineurial cells, and lung fibroblasts. J Virol **2016**; 90:10527–34.
26. Campbell DE, Raftery N, Tustin R 3rd, et al. Measurement of plasma-derived substance P: biological, methodological, and statistical considerations. Clin Vaccine Immunol **2006**; 13:1197–203.
27. Cohrs RJ, Gilden DH. Prevalence and abundance of latently transcribed varicella-zoster virus genes in human ganglia. J Virol **2007**; 81:2950–6.

28. Andrews NC, Faller DV. A rapid micropreparation technique for extraction of DNA-binding proteins from limiting numbers of mammalian cells. Nucleic Acids Res **1991**; 19:2499.
29. Shimizu F, Schaller KL, Owens GP, et al. Glucose-regulated protein 78 autoantibody associates with blood-brain barrier disruption in neuromyelitis optica. Sci Transl Med **2017**; 5:397.
30. Swanson RA, Ying W, Kauppinen TM. Astrocyte influences on ischemic neuronal death. Curr Mol Med **2004**; 4:193–205.
31. Okada S, Nakamura M, Katoh H, et al. Conditional ablation of Stat3 or Socs3 discloses a dual role for reactive astrocytes after spinal cord injury. Nat Med **2006**; 12:829–34.
32. Herrmann JE, Imura T, Song B, et al. STAT3 is a critical regulator of astrogliosis and scar formation after spinal cord injury. J Neurosci **2008**; 28:7231–43.
33. Hara M, Kobayakawa K, Ohkawa Y, et al. Interaction of reactive astrocytes with type I collagen induces astrocytic scar formation through the integrin-N-cadherin pathway after spinal cord injury. Nat Med **2017**; 23:818–28.
34. Jensen DD, Lieu T, Halls ML, et al. Neurokinin 1 receptor signaling in endosomes mediates sustained nociception and is a viable therapeutic target for prolonged pain relief. Sci Transl Med **2017**; 9:eaal3447.
35. Gaddipati S, Rao P, Jerome AD, Burugula BB, Gerard NP, Suvas S. Loss of neurokinin-1 receptor alters ocular surface homeostasis and promotes an early development of herpes stromal keratitis. J Immunol **2016**; 197:4021–33.
36. Svensson A, Kaim J, Mallard C, et al. Neurokinin 1 receptor signaling affects the local innate immune defense against genital herpes virus infection. J Immunol **2005**; 175:6802–11.
37. Muñoz M, Rosso M, Pérez A, et al. The NK1 receptor is involved in the antitumoural action of L-733,060 and in the mitogenic action of substance P on neuroblastoma and glioma cell lines. Neuropeptides **2005**; 39:427–32.
38. Muñoz M, Rosso M, Coveñas R, Montero I, González-Moles MA, Robles MJ. Neurokinin-1 receptors located in human retinoblastoma cell lines: antitumor action of its antagonist, L-732,138. Invest Ophthalmol Vis Sci **2007**; 48:2775–81.
39. Muñoz M, González-Ortega A, Rosso M, et al. The substance P/neurokinin-1 receptor system in lung cancer: focus on the antitumor action of neurokinin-1 receptor antagonists. Peptides **2012**; 38:318–25.
40. Muñoz M, González-Ortega A, Coveñas R. The NK-1 receptor is expressed in human leukemia and is involved in the antitumor action of aprepitant and other NK-1 receptor antagonists on acute lymphoblastic leukemia cell lines. Invest New Drugs **2012**; 30:529–40.
41. Rosso M, Robles-Frías MJ, Coveñas R, Salinas-Martín MV, Muñoz M. The NK-1 receptor is expressed in human primary gastric and colon adenocarcinomas and is involved in the antitumor action of L-733,060 and the mitogenic action of substance P on human gastrointestinal cancer cell lines. Tumour Biol **2008**; 29:245–54.
42. Burmeister AR, Johnson MB, Chauhan VS, et al. Human microglia and astrocytes constitutively express the neurokinin-1 receptor and functionally respond to substance P. J Neuroinflammation **2017**; 14:245.
43. Muñoz M, Muñoz MF, Ayala A. Immunolocalization of Substance P and NK-1 receptor in ADIPOSE stem cells. J Cell Biochem **2017**; 118:4686–96.